Journal of Science: Advanced Materials and Devices xxx (2016) 1–13

Contents lists available at ScienceDirect

Journal of Science: Advanced Materials and Devices

journal homepage: www.elsevier.com/locate/jsamd

Review article

A review on organic spintronic materials and devices: I. Magnetic field effect on organic light emitting diodes

Rugang Geng, Timothy Tyler Daugherty, Kevin Do, Hoang Mai Luong, Tho Duc Nguyen*

Department of Physics and Astronomy, The University of Georgia, Athens, GA 30602, USA

ARTICLE INFO

Article history:
Received 19 May 2016
Accepted 20 May 2016
Available online xxx

Keywords:
Organic spintronics
Organic light emitting diodes
Spin dynamics
Organic magnetoresistance
Magnetic field effect

ABSTRACT

Organic spintronics is an emerging and potential platform for future electronics and display due to the intriguing properties of organic semiconductors (OSCs). For the past decade, studies have focused on three types of organic spintronic phenomena: (i) magnetic field effect (MFE) in organic light emitting diodes (OLEDs), where spin mixing between singlet and triplet polaron pairs (PP) can be influenced by an external magnetic field leading to organic magnetoresistive effect (OMAR); (ii) magnetoresistance (MR) in organic spin valves (OSVs), where spin injection, transport, manipulation, and detection have been demonstrated; and (iii) magnetoelectroluminescence (MEL) bipolar OSVs or spin-OLEDs, where spin polarized electrons and holes are simultaneously injected into the OSC layer, leading to the dependence of electroluminescence intensity on relative magnetization of the electrodes. In this first of two review papers, we present major experimental results on OMAR studies and current understanding of OMAR using several spin dependent processes in organic semiconductors. During the discussion, we highlight some of the outstanding challenges in this promising research field. Finally, we provide an outlook on the future of organic spintronics.

1. Introduction

Spin electronics or spintronics has attracted considerable research and technological attention for over three decades [1,2]. It has already revolutionized magnetic hard-disk technology and will continue to play a central role in the development of new information technology. The concept of electron spin was originally introduced by Wolfgang Pauli in 1924 after the crucial experimental discovery of the quantization of the intrinsic angular momentum, or spin, of silver atoms by Walther Gerlach and Otto Stern in 1922 [3,4]. Similar properties were later found in various atomic nuclei [5]. However, the potential of using the electron's spin degree of freedom in electronic devices was not realized until in 1975 by Jullière through the discovery of the tunneling magnetoresistance (TMR) in the ferromagnet (FM)/insulator/superconductor magnetic tunnel junction (MTJ) [1,6–8]. It was only a couple of years after Tedrow et al. showed spin polarization in the ferromagnetic/insulator tunnel barrier [7,8]. In the late eighties, Fert [9] and Grünberg [10] independently showed the diffusion of spin polarized carriers through a non-magnetic (NM) metal layer in contact with FM layers for an in-plane current and called this effect the giant magnetoresistance (GMR), the discovery for which they were awarded a Nobel Prize in 2007. The explanation of GMR in the FM/NM/FM layered structure was based upon spin dependent scattering. This discovery revolutionized modern information storage and paved a way for future spin-logic devices. After these innovative discoveries, research in this field accelerated impressively and advanced to a range of different materials and a number of techniques to verify the successful injection and transport of the spin polarized carriers [1,2,11,12]. The effect has been observed in a variety of material combinations such as FM films, FM/anti-FM coupled layers, or FM semiconductors as the injection/detection electrodes and metal layer, superconductors, inorganic semiconductors, organic semiconductors (OSCs), and insulators including ferroelectric and topological insulators as the spacers [1,2,13–19]. The GMR effect was extensively studied using non-magnetic metallic interlayers and potential applications such as electric switching, magnetic recording, and sensors were suggested and employed [1,2,17]. However, all-metallic spintronic devices imposed restrictions on applications as they are characterized by short spin relaxation times (~picosecond) and are not suitable for coherent spin manipulation [1,2,20]. To overcome these limitations, the spintronics community moved its attention towards hybrid

* Corresponding author.
E-mail address: ngtho@uga.edu (T.D. Nguyen).
Peer review under responsibility of Vietnam National University, Hanoi.

http://dx.doi.org/10.1016/j.jsamd.2016.05.002

devices with semiconductors sandwiched in between the FM layers and continued advancing to a range of semiconducting materials [2,15,21–23].

Organic semiconductors have appeared as one of the newest spacers for spintronic devices; having been employed for just about a decade. However, the OSC-based research on other electronic devices such as organic light emitting diodes (OLEDs) [24–26], organic solar cells [27,28], and organic field effect transistors [29,30] has been of central interest for over three decades. In fact, OLEDs have already revolutionized the modern display industry, and spin-dependent devices such as organic spin valves (OSVs), OLED-based magnetic sensors, and spin-OLEDs are under intensive study to achieve their new avenues [31–33]. This increasing interest in organic electronics is due to several distinctions over their inorganic counterparts [20–22,34,35] including its rich physics, flexible chemistry, cost efficiency, and potential applications in new generations of electronic devices. Electronically, the band theory explains the electronic transport in inorganic semiconductors, while charge transport in OSCs is much more complicated. This is because organic molecules are electrically conductive as a result of the delocalization of π-electrons caused by conjugation over all or part of the molecule. When being doped by a proper dopant, these materials have conductivity levels ranging from insulators to conductors [36]. Since the intermolecular (van der Waals) forces in organic materials are much weaker than the covalent and ionic bonds of inorganic crystals, organic materials are less rigid than inorganic substances. A moving charge carrier in OSCs is, therefore, able to locally distort its host material. Since strong electron-phonon coupling occurs in organic materials, the electron can be treated as a quasi-particle, namely a polaron. Since the OSC is highly disordered, polaron transport is governed by a process called hopping with very low mobility [37]. This might be a favorable condition for a large polaron pair recombination rate without the need of using a p-n semiconducting junction structure [24–26]. Spintronically, the inorganic semiconductors contain heavy atoms giving rise to a large spin-orbit coupling (SOC), which is a response of the electron spin degree of freedom to its orbital environment. The strength of the SOC in solids depends upon the nature of the orbital wavefunctions of electrons and the material's structure [38]. In the case of the hydrogen-like electron wavefunction, the SOC is proportional to the fourth order of the atomic number. If the probability of finding an electron around the nuclei is taken into account, the effective strength is estimated to vary with the second order of the atomic number [39]. Therefore, the OSCs (usually small molecules or π-conjugated polymers, see Fig. 1) possess a weaker SOC as they are composed of light molecular weight materials such as carbon and hydrogen. The transport from π-orbital electrons also further suppresses the SOC and the hyperfine interaction (HFI), which is the interaction between the spins of an electron and its adjacent nuclei, in these materials [20,40]. Therefore, a net of the spin scattering sources in the OSCs is very weak so that their spin relaxation time (in the μs range) is several orders of magnitude larger than in inorganics (in the ns range) [2]. This makes the OSCs promising candidates for coherent spin manipulation logic devices, such as spin transistors [41]. The first organic spintronic sandwiched device, LSMO($La_{2/3}Sr_{1/3}MnO_3$)/T_6/LSMO in a lateral structure was designed and tested by Dediu et al. in 2002 [21]. They observed a large change in resistance of the structure at room temperature due to an applied magnetic field that suggested an injection of spins into T_6 (see Fig. 1 for its structure) OSCs. In 2004, Xiong et al. [22] demonstrated the first spin valve effect in vertical organic spin-valve (OSV) devices by sandwiching Alq_3 (see Fig. 1 for its structure) in between LSMO and thin cobalt (Co) layers. Following these novel works, much effort has been made in proving [42–44] and disproving [45–47] the possibility of spin injection in OSCs, optimizing their injection and detection efficiency, and understanding the spin transport properties in the hybrid devices of metallic FM electrodes and OSC interlayers [20,34,35,42,48–51]. In addition to the spin valve effect, a different type of MR effect in the OLED devices, the so-called organic magnetoresistance (OMAR), has also been observed in a range of OSCs [52–61]. In contrast to MR in OSVs, which is thought to give the largest MR response when electron spin-related interactions in the organic interlayer are minimized, OMAR in OLEDs is an intrinsic property found in most OSC materials and it relies on the existence of HFI and/or SOC fields and their randomization [53,55,62–67]. These interactions induce electron spin flips, leading to the interconversion between singlet and triplet polaron pairs (either excitons or bipolarons), which have a direct effect on the electroluminescence (EL) and conductivity of the device. Recent experiment on OLEDs made by an OSC blend predicts that the difference in g-value of positive and negative polarons located in the donor and acceptor, respectively, might cause spin mixing between singlet and triplet states [68,69]. OMAR in OLEDs may be considered as an example of a much broader research field that deals with magnetic-field-effects (MFE) in Physics [70], Chemistry and Biology [71,72]. Recently, there has been interest in the bipolar OSV or spin-OLED structure, where spin polarized electrons and holes are injected from the FM cathode and FM anode, respectively. The EL of the device depends on the relative magnetization of the electrodes. In ideal conditions, the device can reach 50% EL internal quantum efficiency (IQE) for parallel magnetization states and 0% EL IQE for the anti-parallel magnetization states. Excellent reviews on the different aspects of organic spintronic devices can be found in the literature [20,32,35,40,50,52,73–78].

In this first of two review papers, we overview the progress of OMAR study in OLEDs over a decade long period with an outlook in this promising field. In particular, we give the basic operating principle of organic light emitting diodes, the experimental advances over the period, and the major models well established in this field. Finally, we summarize the report give an outlook for the advancement of the research in this promising field.

2. Organic light emitting diodes

A typical OLED is composed of an OSC layer situated between two non-magnetic electrodes, the anode (cathode) made by high (low) work-function materials, all deposited onto a glass substrate (Fig. 2a). Fig. 2b shows work functions of common metals and the highest occupied molecular orbital (HOMO) and the lowest unoccupied molecular orbital (LUMO) energy levels of polyfluorene (PFO) (see Fig. 1 for its structure). During operation, a voltage is applied across the device. A current of negative/positive polaron (P^-/P^+) flows through the device, as electrons (holes) are injected into the LUMO (HOMO) of the organic layer at the cathode (anode). Since organic materials normally possess a small electrical permittivity, the strong electrostatic forces between the P^- and P^+ bring them together. These materials first form a polaron pair (*PP*) exciton; a loosely bound state of the P^- and P^+ with negligible exchange interaction at a distance of several nanometers. Because polarons are fermions with spin ½, either in up-spin (↑) or down spin (↓) state, a *PP* may be in a singlet state PP_S ($\uparrow\downarrow - \downarrow\uparrow$) or a triplet state PP_T of either $\uparrow\uparrow$, $\downarrow\downarrow$, or ($\uparrow\downarrow + \downarrow\uparrow$), depending on how the spins of P^+ (the first arrow) and P^- (the second arrow) have been combined. Statistically, three triplet *PP* will be formed for each singlet *PP*. The free carriers and *PP* excitations are in dynamic equilibrium in the device active layer, which is determined by the balance between positive and negative polaron densities, the processes of *PP* formation/dissociation and recombination via intra-chain excitons. The steady state *PP* density depends on the PP_S and PP_T, the "effective rate constant", *k*, which is the sum of the

Please cite this article in press as: R. Geng, et al., A review on organic spintronic materials and devices: I. Magnetic field effect on organic light emitting diodes, Journal of Science: Advanced Materials and Devices (2016), http://dx.doi.org/10.1016/j.jsamd.2016.05.002

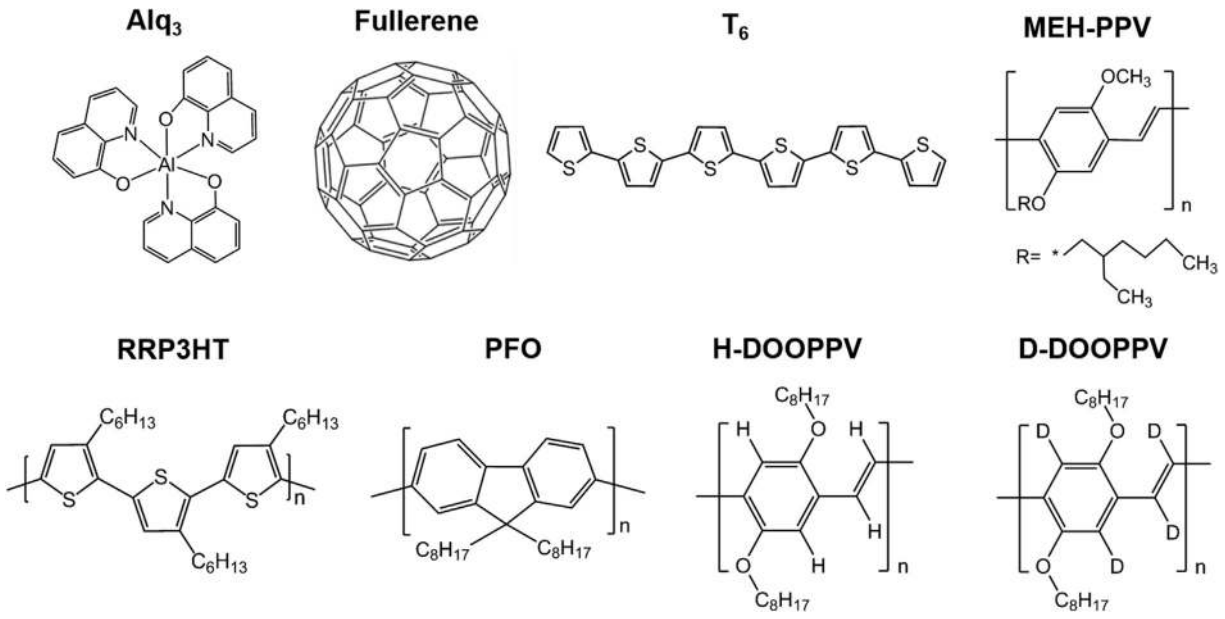

Fig. 1. Chemical structure of some organic semiconductors including small molecules and π-conjugated polymers: tris(8-hydroxyquinolinato)aluminium (Alq_3), Fullerene, sexithienyl (T_6), poly [2-methoxy-5-(2-ethylhexyloxy)-1,4-phenylenevinylene](MEH-PPV), regioregular Poly (3-hexylthiophene-2,5-diyl) (RRP3HT), poly (9,9-dioctylfluorenyl-2,7-diyl (PFO), protonated poly (dioctyloxy)phenylenevinylene (H-DOOPPV), deuterated poly (dioctyloxy)phenylenevinylene (D-DOOPPV).

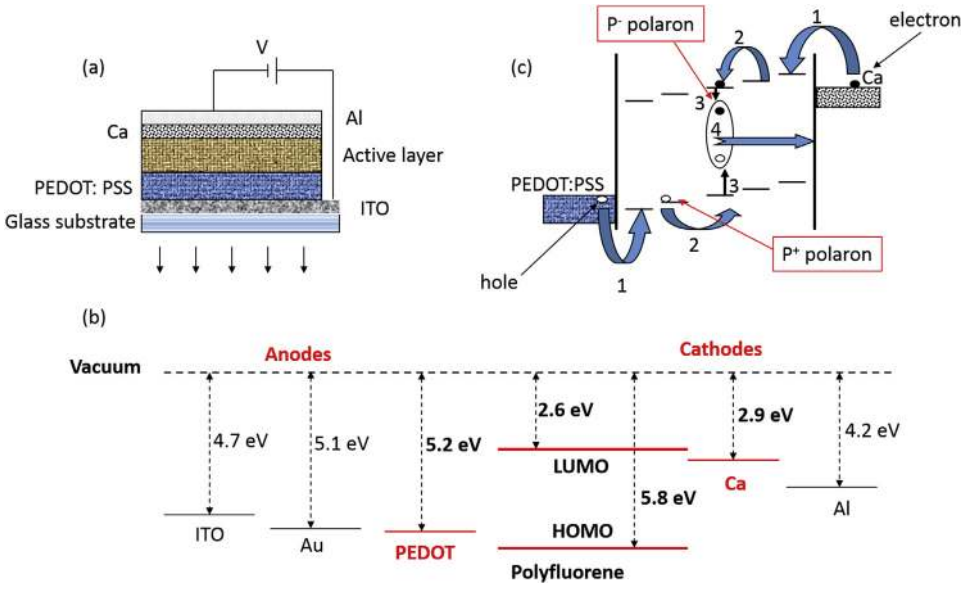

Fig. 2. (a) Device layout of a typical OLED. (b) Work functions of common metals used in making electrodes and typical HOMO, LUMO energies of an organic semiconductor, polyfluorene (PFO). The left materials are typically used as hole injection electrodes, while the right ones are usually used as electron injection electrodes. (c) Working principle of OLED: four important processes are shown: (1) charge injection; (2) charge transport; (3) recombination of positive and negative polarons to form loosely bound PP; and (4) exciton formation and emission.

formation, the dissociation and recombination rate constants, as well as the triplet-singlet mixing via the intersystem crossing (ISC) interaction. If the effective rates k_S for PP_S and k_T for PP_T are not identical to each other, any disturbance of the singlet-triplet mixing rate, such as by triplet–triplet annihilation, triplet-polaron interaction, hyperfine interaction from adjacent hydrogens [72], spin orbit field [79] from incorporated heavy metals, or an applied magnetic field, B, would perturb the dynamical steady state equilibrium that results in a change of emission efficiency and polaron density. In principle, there are three distinct mechanisms for the emission efficiency: (i) direct fluorescence from the singlet exciton that limits the IQE to about 25% depending on the singlet radiative recombination rate and the ISC rate; (ii) phosphorescence from triplet excitons using incorporated heavy metals that give IQE up to 100%; and (iii) delayed fluorescence that can be from either triplet–triplet annihilation or thermally-assisted up-conversion of triplet to singlet excitons. The triplet–triplet annihilation gives weak delayed fluorescence due to a small portion of triplet–triplet pairs annihilating to excited singlet excitons, while the thermally-assisted up-conversion would give up to 100% IQE depending on the energy gap between singlet and triplet excitons relative to the thermal energy. The first two emission mechanisms have been

Please cite this article in press as: R. Geng, et al., A review on organic spintronic materials and devices: I. Magnetic field effect on organic light emitting diodes, Journal of Science: Advanced Materials and Devices (2016), http://dx.doi.org/10.1016/j.jsamd.2016.05.002

explored in the past three decades. Recently, highly efficient OLEDs with thermally activated delayed florescence (TADF) have been reported by Adachi's group [80]. In TADF materials, there is little overlap between the orbital wavefunctions of localized positive polarons in the HOMO level of a donor and localized negative polarons in the LUMO level of an acceptor whose locations can be designed in a single molecule (in the case of exciton-based TADF materials) or different molecules (in the case of exciplex-based TADF materials). Consequently, the singlet and triplet excitons/exciplexes have small energy gaps due to a small exchange energy, J, of typically less than 200 meV [81]. In principle, the smaller the J value, the larger the TADF intensity. Therefore, thermal energy plays an important role to increase the up-conversion rate from triplet to singlet excitons/exciplexes. The internal EL quantum efficiency of such OLEDs can reach 100% without the need of using incorporated heavy metals [80]. Fig. 2c shows four main steps of the working principle of an OLED.

3. Advances in experimental parts of magnetic field effect in OLEDs

In 2003, Kalinowski et al. showed that EL and current density can be modulated by a few percent in OLEDs made of small molecules, such as Alq_3, by application of a small magnetic field of about 100 mT [62,82]. Later, Wohlgenannt et al., demonstrated a very large magnetoresistance of up to 30% at the same characteristic magnetic field in PFO-based OLEDs [83]. The effect was dubbed OMAR. In this section, the term MFE or OMAR will be used interchangeably for both magnetoconductance (MC) and magneto electroluminesscence (MEL). It is worth noting that the magnetic field effect on photocurrent of several percent in poly (phenylene vinylenes) and its derivatives, an analogous effect with OMAR, was observed by Frankevich et al., in 1992 [84]. In such devices, the electron density and the hole density are assumed to be the same. The MC and MEL responses are defined, respectively, via

$$MC(B) = \Delta I(B)/I(0) = \frac{I(B) - I(B=0)}{I(B=0)} \quad \text{and}$$
$$MEL = \Delta EL(B)/EL(0) = \frac{EL(B) - EL(B=0)}{EL(B=0)}, \tag{1}$$

where ΔI and ΔEL are the field induced changes in the current and EL intensity, respectively. Fig. 3 shows the large MEL and MC (essentially an inverse of OMAR) magnitudes of an Alq_3-based OLED [85]. The MEL (MC) response may reach up to 60% (30%) at B ~100 mT. It is surprising that a small magnetic field, with Zeeman splitting on the order of ~μeV, can significantly alter the EL and conductivity of the device at room temperature where thermal energy, ~26 meV, is dominate. Therefore, MFE must be caused by effects on spins in a thermal nonequilibrium situation. Recently, there has been interest in studying the magnetic field effect in TADF-based OLEDs [69,86]. The MEL and MC of about 4000% and 1000%, respectively, have been achieved in such OLEDs in a certain device operation [69]. This makes MFE in OLEDs very attractive for various applications.

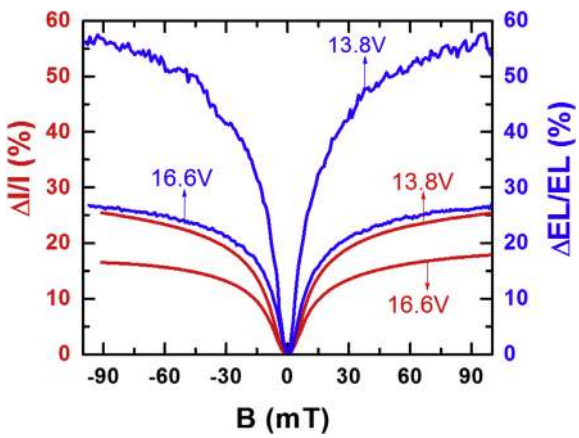

Fig. 3. Magneto-conductance (ΔI/I) and magneto-electroluminescence (ΔEL/EL) in an OLED device made of ITO (30 nm)/PEDOT (~100 nm)/Alq_3 (~100 nm)/Ca (~30 nm)/Al (30 nm) with two different bias voltages at room temperature. Reproduced with permission [85].

Now, we briefly summarize the main experimental results of MFE in the following sections:

(i) Since OMAR in the conventional OLEDs is generally insensitive to OSC thickness, OMAR is an effect associated with the bulk resistance of the layer, rather than the OSC/electrode interfacial resistance [54]. However, a recent study of OMAR on TADF-based OLEDs shows an order of magnitude increment in OMAR magnitude when the thickness increases from 50 nm to about 180 nm [69].

(ii) OMAR is essentially independent of the magnetic field direction and is insensitive to the ambient temperature [54]. We note that recently Wagemans et al. [49] found that OMAR in OLEDs has a tiny variation when magnetic field B changes from perpendicular direction to parallel direction to the device current. This tiny change and its mechanism will not be discussed in this review.

(iii) OMAR can be of positive or negative sign, depending on material and/or operating conditions of the devices [54,59,83,87]. Fig. 4 shows the magnetoresistance reversal of OLEDs made with RRP3HT and T_6 (see Fig. 1 for their chemical structures), where the sign of the magnetoresistance is dependent on temperature (Fig. 4a) and applied voltage (Fig. 4b).

(iv) The magnitude OMAR can be an order of magnitude larger when trap states are introduced in the materials by either electrical conditioning or by X-ray illumination (Fig. 5a) [88,89]. The signature of the presence of trap states is the strong reduction in device conductivity and electroluminescence intensity. In this case, the polarons are more localized, leading to the longer excited state lifetimes that would allow more time for spin mixing between singlet and triplet states. Interestingly, in the TADF materials, where the positive and negative polarons are strongly localized in the donor and acceptor units, respectively, a much larger MEL and MC of about 100% has been observed (Fig. 5b) [86]. When the device is electrically conditioned, the stronger polaron localization significantly enhances OMAR up to a few thousand percent (Fig. 5c) [69]. We note that in most cases, a larger OMAR magnitude is always accompanied by a larger OMAR half width at half maximum (HWHM).

(v) OMAR generally obeys the empirical laws $\Delta I(B)/I \approx B^2/(B^2 + B_0^2)$ (Lorentzian shape) or $\Delta I(B)/I \approx B^2/(|B| + B_0)^2$ (non-Lorentzian shape) depending on the material and applied voltages [54], where B_0 of about 5 mT scales with HFI/SOC strength (Fig. 6) [48,63,65]. In many other cases, such as described in Fig. 4 the OMAR response cannot be fit by a single empirical function. This scenario was discussed before by Wang et al. [60] Gillin et al. found that OMAR can be better fit by the sum of two or three Lorentzian functions (see the olive line in Fig. 6) [90,91]. This suggests that there may be more than one OMAR mechanism involved in the effect depending on OSC materials, device fabrication and operating condition [60,90].

Please cite this article in press as: R. Geng, et al., A review on organic spintronic materials and devices: I. Magnetic field effect on organic light emitting diodes, Journal of Science: Advanced Materials and Devices (2016), http://dx.doi.org/10.1016/j.jsamd.2016.05.002

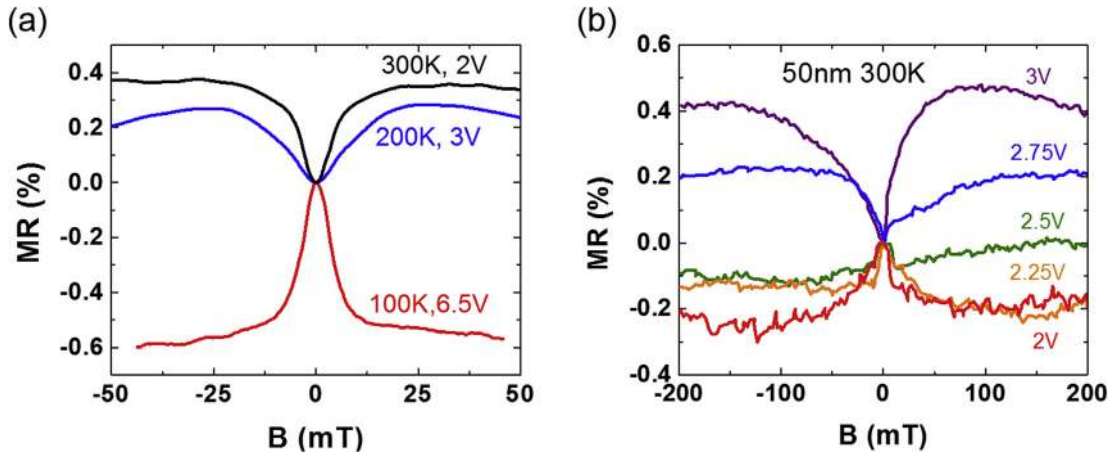

Fig. 4. Magnetoresistance of (a) RRP3HT-based OLED at different temperatures [54] and (b) α-T_6-based OLED at various voltages at room temperature [87]. Reproduced with permission.

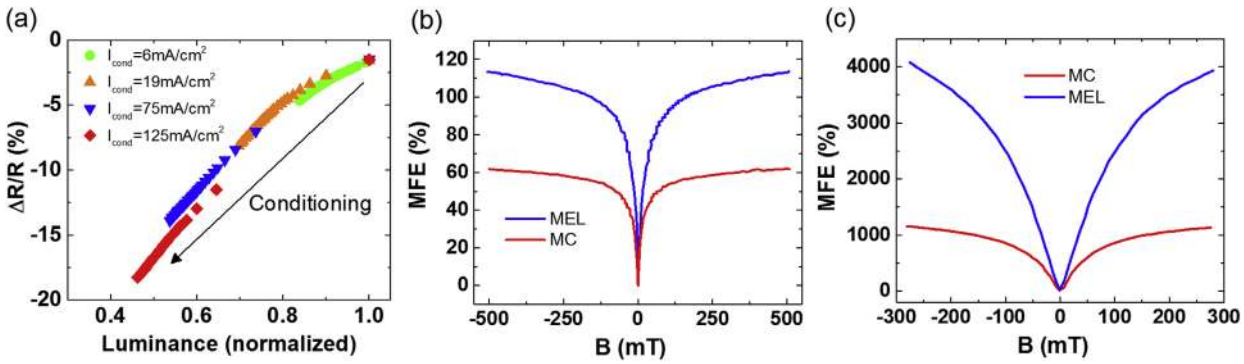

Fig. 5. Organic magnetoresistance (OMAR) under electrical condition. (a) magnetoresistance in MEH-PPV based OLEDs with electrical conditioning [88]. (b) MC and MEL in an exciplex based OLEDs [86] and (c) MC and MEL after conditioning [69]. Reproduced with permission.

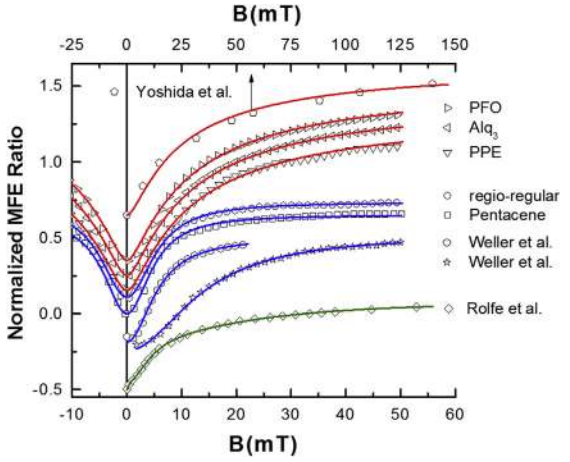

Fig. 6. Normalized OMAR traces fitted by using different empirical laws. The solid curves are fits using Lorentzian function of forms $B^2/(|B| + B_0)^2$ (red lines) [65], $B^2/(B^2 + B_0^2)$ (blue lines) [65], and triple Lorentzian function (olive line) [91]. Reproduced with permission.

(vi) In a conventional polymer, the magnetic field value, $B_{1/2}$, at HWHM of the OMAR scales by the effective HFI strength of the material, which is influenced by the HFI strengths of positive and negative polarons [48]. Fig. 7a shows the MEL response of two OLED devices based on H- and D-DOOPPVs (see Fig. 1 for the chemical structures) with the same thickness d_f, measured at the same bias voltage, V; a very similar MC response was also measured simultaneously (Fig. 7b). The MEL and MC responses are narrower in the D-DOOPPV device; in fact, the field, $B_{1/2}$, for the MEL in the H-DOOPPV device is about twice as large as in the D-DOOPPV device [48]. Interestingly, $B_{1/2}$ increases with V (inset of Fig. 7a) [60]. In fact, $B_{1/2}$ increases almost linearly with the device electric field, $E = (V\text{-}V_{bi})/d_f$, where V_{bi} is the built-in potential in the device that is related to the onset bias voltage where EL and MEL are observed [58,92]. It is consistently observed that $B_{1/2}(H) > B_{1/2}(D)$ for devices with the same value of the electric field, E (inset of Fig. 7a). We note that similar studies have been done using hydrogenated Alq_3 (H-Alq_3) and deuterated Alq_3 (D-Alq_3) [93,94]. However, it is surprising that MC is found to be isotope independent while the MEL response in H-Alq_3 is nearly 1.5 times wider [93,94]. The disparity between the isotope sensitivity of the MC and MEL responses in Alq_3 indicates that the HFI in the MC response is overwhelmed by another spin mixing mechanism such as the polaron-triplet scattering, which does not have a direct effect from HFI [94]. The other possibility is that OSC strength originated by the Al atom in Alq_3 materials might be comparable with the HFI strength, which further complicates the effect. This scenario is supported by the observation of phosphorescence in Alq_3 films [95]. It is worth noting that the MC in fullerene-based OLEDs was not observable due to

Please cite this article in press as: R. Geng, et al., A review on organic spintronic materials and devices: I. Magnetic field effect on organic light emitting diodes, Journal of Science: Advanced Materials and Devices (2016), http://dx.doi.org/10.1016/j.jsamd.2016.05.002

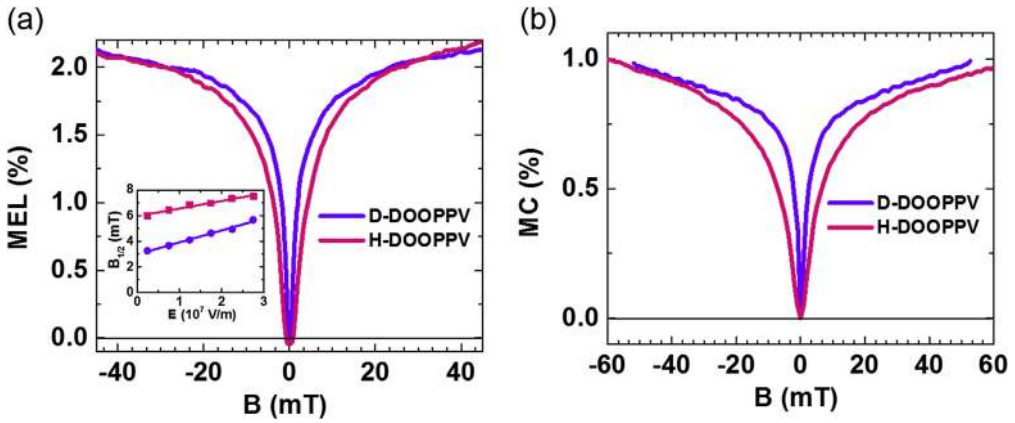

Fig. 7. Isotope dependence of (a) magneto-electroluminescence (MEL) and (b) maneto-conductivity (MC) responses in OLEDs based on D- and H-DOOPPVs measured at bias voltage $V = 2.5$ V and at room temperature [48]. Inset in (a) shows the field, $B_{1/2}$ for the two polymers, plotted versus the applied bias voltage, V, with linear fits, where V is given in terms of the internal electric field in the polymer layer, $E = [V\text{-}V_{bi}]/d_r$. Reproduced with permission.

the absence of nuclear spins [96]. In addition, Malisa et al. recently observed a direct coupling between the electrical current and nuclear spins in OLEDs [97]. This additional evidence clear doubts about the crucial role of HFI in the observation of large OMAR effect.

(vii) Relatively small and negative MC was found in unipolar devices that usually do not show EL at low applied voltages [58,60,63]. Fig. 8a shows normalized MC of an electron-only device and a hole-only device made with MEH-PPV (see Fig. 1 for its structure). Its chemical structure is shown in Fig. 1. The MC magnitude in the unipolar device is relatively smaller than that in the bipolar device. In addition, the MC of the electron-only device shows much larger magnitude and $B_{1/2}$ than in the hole-only device. The result implies that the HFI strength of electrons is larger than that of holes in MeH-PPV polymers.

(viii) The magnetic field response of OMAR universally shows a sign reversal (characterized by B_m, where OMAR is minimum) at ultra-small $|B| < 1$–2 mT probably due to the interplay of the hyperfine and Zeeman interactions on carrier spins [63]. Fig. 9a and b show that the MEL and MC in OLEDs have yet another component at low B, dubbed "ultra-small-field MEL/MC" or USMEL/USMC, which has an opposite sign to that of the positive MEL (MC) at higher magnetic fields. A similar low-field component was also observed in some biochemical reactions [98] and anthracene crystals [99] with likely the same underlying mechanism as in OLED devices. The USMEL (USMC) component might also be due to the HFI, since its width in the large field effect (see Fig. 7) is isotope dependent; and it is observed that the dip in the USMEL response occurs at $B_m \sim 0.7$ mT in H-DOOPPV, whereas it is at $B_m \sim 0.2$ mT in the D-DOOPPV. The USMFE response is not limited to bipolar devices. In Fig. 8b we show the magnetic field response, USMC(B), of hole-only and electron-only MEH-PPV unipolar devices. Similar responses were also measured for DOOPPV devices [64]. The high-field MC in unipolar devices is *negative* (Fig. 8a) [60] and thus the USMFE response here appears as a 'negative-to-positive' sign reversal with a *maximum* at $B_m \sim 0.8$ mT for the electron-only device and $B_m \sim 0.1$ mT for the hole-only device (Fig. 8b). This implies that the HFI strength of the electron-polaron is larger than that of the hole-polaron in MeH-PPV. This is consistent with smaller a_{HF} for hole-polaron than for electron-polaron in MEH-PPV shown in Fig. 8a, which is in agreement with recent measurements using transient spin response [100]. We therefore conclude that B_m increases with the HWHM in unipolar devices in a similar fashion to bipolar devices [63]. This finding suggests that one can obtain the effective HFI of electrons or holes separately in OSC by MFE in unipolar devices rather than by magnetic resonance techniques.

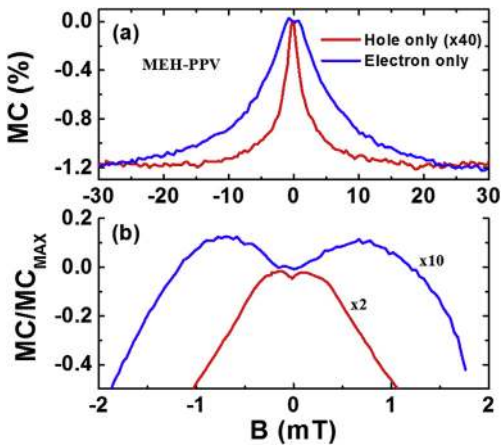

Fig. 8. Normalized MC(B)/USMC(B) response for (a) $|B| < 30$ mT, and (b) $|B| < 2$ mT in hole- and electron-only *unipolar* diodes based on MEH-PPV, measured at room temperature and $V = 3$ V and 20 V, respectively. The USMC(B) responses are somewhat shifted in (b) for clarity [63]. Reproduced with permission.

We note that OMAR has been studied in OSCs containing heavy metals [53,55,101]. Since the SOC in this case is quite large compared to HFI strength, the OMAR response is normally quenched and its HWHM is significantly broader [53,55,101]. In addition to intrinsic SOC, recent study shows that the curvature-enhanced SOC might also play an important role on electron spin dynamics in organic substances [102]. In the following section, we only focus our discussion on OMAR mechanisms in conventional OSCs only where HFI dominates.

4. Advances in modeling of magnetic field effect in OLEDs

In general, the current density of the device, j, can be written using the Drude model of electrical conductivity:

$$j = en\mu E = \sigma E, \tag{2}$$

where e is elementary charge, n is density of negative and positive polarons, μ is carrier mobility, σ is the conductivity, and E is the electric field inside the device, which is insensitive to applied

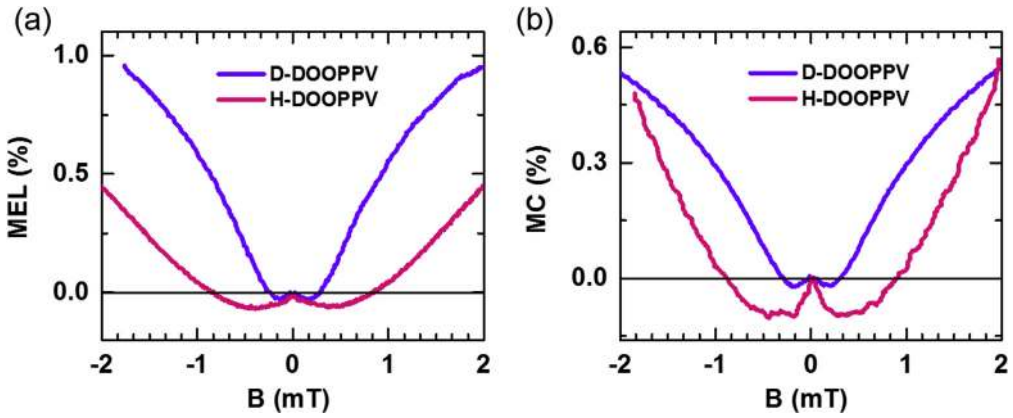

Fig. 9. Room temperature MEL (MC) response of D- and H-DOOPPVs (solid and dash lines, respectively) measured at bias voltage $V = 2.5$ V, plotted for $|B| < 3$ mT [48,63]. Reproduced with permission.

magnetic field. Therefore, the large magneto-current (or magneto−conductivity) can be explained by a magnetic field dependent carrier density, n, and/or magnetic field dependent mobility, μ.

Based on this general argument, various models have been put forth to explain OMAR in OLED devices [55,57,59,60,63,103]. Four outstanding models have been proposed to explain OMAR at the field range less than 100 mT:

(i) The bipolaron mechanism, which treats the spin-dependent formation of doubly occupied sites (bipolarons which are polaron pairs of the same sign) during the hopping transport through the organic film [57,104,105]. Due to the strong exchange interaction between the on-site polarons, a singlet bipolaron is more energetically favorable to form than a triplet bipolaron. A magnetic field such as from HFI field or applied magnetic field can influence the singlet bipolaron formation. Consequently, the hopping mobility is altered by an applied magnetic field.

(ii) The loosely-bound *PP* pair model, where the interconversion between singlet and triplet density via HFI-based ISC is affected by an applied magnetic field [55,62,63]. The singlet density increases by the suppression of the triplet density and vice versa. As a result, it affects device conductivity via e-h pair dissociation and EL via singlet radiative recombination. This model supports the assumption that the magnetic field enhances the charge density and thereby enhances the current density.

(iii) The triplet-exciton polaron quenching model (TPQ), which relies on the spin-dependent reaction between a triplet exciton and a polaron (either a free or trapped) [56,59]. The applied magnetic field can affect the triplet exciton density via the ISC process. Furthermore, it can influence the spin mixing between the triplet excitons and polarons, therefore changing the mobility [103] and density [59] of mobile polarons in the device.

(iv) The Δg mechanism relies on the different gyromagnetic factor between positive polaron (g^+) and negative polaron (g^-). Since the negative and positive polaron spins precess with different Larmor frequencies, the singlet and triplet state mixing rate is proportional to $(g^+ - g^-)\cdot B = \Delta g \cdot B$. [60] The Δg mechanism becomes more effective at high magnetic field [68]. The model explains OMAR based on the MFE on the charge density of the device.

In general, the first three models are constructed based on the HFI between the spin ($s = ½$) of the injected charge carriers and the proton nuclear spins located at the chemical backbone of the active layer. The last three mechanisms are based on exciton formation, where negative/positive PP formation is necessary. The general understanding for all OMAR mechanisms is that the spin mixing between pairs of either the same sign or opposite signs becomes less (more) effective as the magnetic field increases for the HFI-based mechanisms (Δg mechanism), thereby inducing OMAR. In the following sections, the fundamental ideas behind the mechanisms are presented.

4.1. Bipolaron model

Bobbert et al. [57] considered the effect of a magnetic field on the hopping probability of a polaron from a localized state at site α to another nearest localized state at site β, which is already occupied by a like-charge polaron (Fig. 10). In the previous section, we pointed out that oppositely charged polarons can form excitons and may eventually recombine to emit light. However, two like-charge polarons can form a bipolaron; a state where the correlation energy between the pair and the lattice deformation lowers the formation energy. The on-site charge exchange interaction requires that the bipolaron is a spin singlet. The bipolaron formation will be “spin-blocked” if the two polarons have the same spin component along the common quantization axis. In addition, these polarons are exposed to a local hyperfine field produced by the adjacent nuclear spins, which can be treated as a randomly oriented classical field B_{hf}. The total field at a site α is then $B_{total;\alpha} = B + B_{hf;\alpha}$, where B is the applied magnetic field (Fig. 10). The hopping therefore occurs between energy eigenstates corresponding to the local net magnetic fields randomly oriented at the two sites where the spin precession frequency is assumed to be larger than the hopping frequency. The singlet probability is now given by

$$P = \frac{1}{4} - \frac{1}{\hbar^2}\boldsymbol{S}_\alpha \cdot \boldsymbol{S}_\beta, \tag{3}$$

where $\boldsymbol{S}_{\alpha/\beta}$ are the classical spin vectors pointing along $\boldsymbol{B}_{total;\alpha/\beta}$, and $\hbar$ is Planck's constant. A straightforward analysis of this formula shows that for $B = 0$ the pairs have an average singlet probability $P = 1/4$, whereas for large field this probability is either equal to zero or one-half for parallel and antiparallel pairs, respectively. Note that the notion of parallel and antiparallel pairs has its usual meaning only for large B; whereas for small B, Bobbert et al. denote “parallel” as a pair whose spins both point “up” or both “down” along the local field axes.

Please cite this article in press as: R. Geng, et al., A review on organic spintronic materials and devices: I. Magnetic field effect on organic light emitting diodes, Journal of Science: Advanced Materials and Devices (2016), http://dx.doi.org/10.1016/j.jsamd.2016.05.002

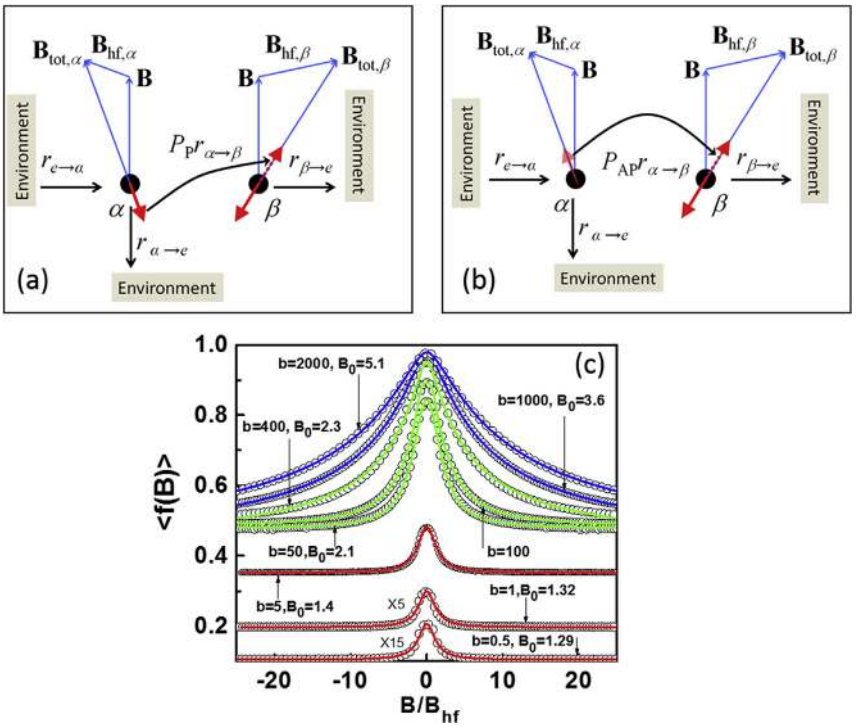

Fig. 10. Bipolaron model as described in the main text, with the red arrow indicating the spin of a polaron present at β (arbitrarily chosen opposite to the local magnetic field) and the red arrows at site α shows the spin of a possible additional polaron for (a) anti-parallel spin hopping and (b) parallel spin hopping. (c) Hyperfine field average of the function $f(B)$ of Eq. (8) for various branching ratios b. The lower three red lines show Lorentzian fits, the upper two blue lines fit to the non-Lorentzian empirical law. The fitting parameters B_0 are shown [57]. Reproduced with permission.

We will now formulate rate equations to describe the hopping transport. Bobbert et al. [57] assumed that the low energy site, β, can permanently hold at least one polaron. A bipolaron can be formed by the hopping of a polaron to an adjacent site, known as the "branching" site, with a rate $P_P r_{\alpha\to\beta}$ (Fig. 10a) or $P_{AP} r_{\alpha\to\beta}$ (Fig. 10b), depending on the orientation of its spin. The model assumes that the electric field is large enough such that dissociation does not occur to α but, at a rate $r_{\beta\to\alpha}$ to other sites, which it considers to be a part of the "environment". The model assumes that polarons enter α with a rate $r_{e\to\alpha}$ by hopping from sites in the environment with equal "parallel" and "antiparallel" spins leading to an influx rate $r_{e\to\alpha}p/2$ into both spin channels, where p is a measure for the average number of polarons in the environment. The model also considers the possibility that a polaron at α directly hops back to an empty site in the environment with a rate $r_{e\to\alpha}$. Neglecting a double occupancy of α and single occupancy of α simultaneously with double occupancy of β, the corresponding rate equations can be straightforwardly written down:

$$\frac{1}{2} r_{e\to\alpha} p - \left(r_{\alpha\to e} + P_P r_{\alpha\to\beta}\right) p_{\alpha P} = 0 \tag{4}$$

$$\frac{1}{2} r_{e\to\alpha} p - \left(r_{\alpha\to e} + P_{AP} r_{\alpha\to\beta}\right) p_{\alpha AP} = 0 \tag{5}$$

$$P_P r_{\alpha\to\beta} p_{\alpha P} + P_{AP} r_{\alpha\to\beta} p_{\alpha AP} - r_{\beta\to\alpha} p_\beta = 0. \tag{6}$$

These equations can be solved for the probability p_β of double occupancy of β, i.e. the presence of a bipolaron:

$$p_\beta = \frac{r_{e\to\alpha}}{r_{\beta\to e}} f(B) p, \tag{7}$$

with

$$f(B) = \frac{P_A P_{AP} + \frac{1}{4b}}{P_P P_{AP} + \frac{2}{b} + \frac{1}{b^2}}, \tag{8}$$

where the B dependence has been absorbed in the function $f(B)$ and $b = r_{\alpha\to\beta}/r_{\alpha\to e}$ is the *"branching"* ratio. In general, the conductivity of the device is proportional to the probability p_β or $f(B)$. Averaging over the directions of the hyperfine fields, one obtains the results for $<f(B)>$ plotted in Fig. 10c for various values of b. For small b the line shape is governed by $<(P_P P_{AP})>$. For large b, a strong dependence on B develops, which now becomes governed by $<1/(P_P P_{AP})>$. These line shapes can be fitted very well with the empirical law, $B^2/(|B| + B_0)^2$ for large b and $B^2/(B^2 + B_0^2)$ for small b. The fitting parameters are shown in Fig. 10c. For intermediate values of b, the line shapes cannot be fit well by either empirical formula. In principle, the bipolaron model can explain the line shape of OMAR response.

Bobbert et al. reinforced this mechanism by employing Monte-Carlo simulations of nearest neighbor hopping on a 30^3 cubic grid of sites with lattice constant a and periodic boundary conditions. The site energies were drawn randomly from a Gaussian density of state and a randomly oriented hyperfine field of strength B_{hf} was attributed to each site. The Miller Abrahams form was used for the hopping rate r, with $r \sim \exp(E_i - E_f)/kT$, where E_f and E_i are the initial and final energies of the configurations before and after hopping. This term includes an energy, eEa, picked up or lost due to hops with or against the applied electric field E, with e being the electronic charge. The short range and long range Coulomb repulsions were also taken into account in the hopping rate. The simulation result shows good agreement in OMAR sign change, magnitude and line shapes [57].

In principle, the bipolaron model can explain various experimental OMAR responses as described in the previous section. In this model, the magnetic field effect on OLEDs can be considered as a combination of two independent effects on electrons and holes

Please cite this article in press as: R. Geng, et al., A review on organic spintronic materials and devices: I. Magnetic field effect on organic light emitting diodes, Journal of Science: Advanced Materials and Devices (2016), http://dx.doi.org/10.1016/j.jsamd.2016.05.002

[58]. The model generally states that the observation of OMAR is independent of device emission. However, the model can not explain the reason why OMAR appears to be large only when the device has a good emission. In addition, bipolaron density has not been spectroscopically observed in OLEDs due to the low current density in the device. Finally, it is not clear how the USMFE could be explained by this model.

4.2. Polaron pair model

There are several versions of PP models used to explain the time evolution of singlet and triplet excitons in organic substances of different configurations, such as in organic solution/films [71] and in OLEDs [62,63,87,106]. Here, we present the complete model proposed by Ehrenfreund et al. [106], which is based on the time evolution of the PP spin sublevels in a magnetic field [63,106]. For bipolar devices, the PP species is the polaron-pair, whereas for unipolar devices the PP species is a π-dimer (i.e. bi-radical, or bipolaron [57,60]). It is assumed that the PP excitations are immobile, hence *PP* diffusion is ignored, but the overall rate of PP decay (e.g. through exciton recombination and/or dissociation into free polarons that contribute to the device current) is taken into account. The steady state singlet fraction of the PP population ("singlet yield", Φ_S) is then calculated from the coherent time evolution of PP wavefunctions subject to the above interactions. The calculated MC (MEL) response is then expressed as a weighted average of the singlet (Φ_S) and triplet (Φ_T) PP yields in an external magnetic field, *B*. The spin Hamiltonian, *H*, includes exchange interaction (EX), HFI and Zeeman terms: $H = H_Z + H_{HF} + H_{ex}$; where $H_{HF} = \sum_{i=1}^{2}\sum_{j=1}^{Ni}[S_i \cdot \tilde{A}_{ij} \cdot I_j]$ is the HFI term, $\tilde{A}$ is the hyperfine tensor describing the HFI between polaron (*i*) with spin S_i (=½) and N_i neighboring nuclei, each with spin I_j, having an isotropic a_{HF} constant; $H_Z = g_1\mu_B BS_{1z} + g_2\mu_B BS_{2z}$ is the electronic Zeeman interaction component; g_i is the g-factor of each of the polarons in the PP species (we chose here $g_1 = g_2$); μ_B is the Bohr magneton; $H_{ex} = JS_1 \cdot S_2$ is the isotropic exchange interaction; and B is along the z-axis. All parameters in the Hamiltonian *H* are given in units of magnetic field (mT). An example of the PP spin sublevels using the Hamiltonian *H* for $N_1 = N_2 = 1$, and I = ½ (overall 16 wavefunctions) is shown in Fig. 11a. Note the multi-level crossings that occur at $B = 0$. Other level crossings appear at larger field, B_{LC}, but those are between mostly triplet sublevels that rarely change the *singlet-triplet* intermixing rate and related PP_S and PP_T populations. The same PP spin sublevels for $N_1 = N_2 = 1$ and I = 1are shown in Fig. 11b.

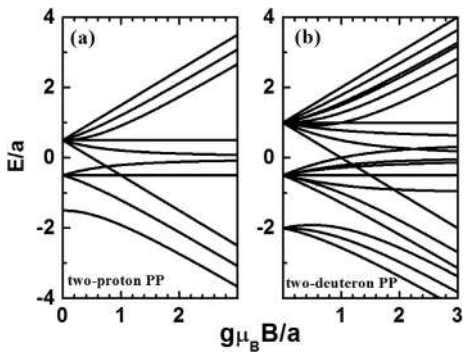

Fig. 11. (a) Energy levels (E) of the 16 spin sublevels of a polaron-pair where each of the two polarons couples to a single proton in the H-DOOPPV (nuclear spin, $I = ½$), based on the spin Hamiltonian that includes HF (*a*), exchange (J_{ex}) and Zeeman interactions, as a function of the applied magnetic field, *B* for the case $J_{ex} << a$. Both E and *B* are given in units of *a*. (b) Same as in (a) but for the 36 spin sublevels of a polaron-pair coupled to two ^{2}H nuclei in the D-DOOPPV ($I = 1$) [48,63]. Reproduced with permission.

The relevant time evolution of the singlet-triplet intermixing that determines the steady state PP_S population is obtained in the model via the time dependent density matrix, $\rho(t)$. Solving the spin Hamiltonian, *H*, for the energies E_n and wavefunctions Ψ_n, we express the time evolution of the singlet population $\rho_S(t)$ as [71,72].

$$\rho_S(t) = Tr\left[\rho(t)P^S\right] = \frac{4}{M}\sum_{m,n=1}^{M}\left|P^S_{mn}\right|^2 \cos\omega_{mn}t, \tag{9}$$

where P^S_{mn} are the matrix elements of the PP_S projection operator, $\omega_{mn} = (E_n - E_m)/\hbar$, and *M* is the number of spin configurations included in the PP species (for I = ½ $M = 2^{N+2}$). In the absence of a spin decay mechanism, Eq. (9) yields for the PP_S steady state population (apart from the rapidly oscillating terms): $<\rho_S\ (t=\infty)> = 4\Sigma_m|P^S_{mm}|^2/M + 4\Sigma_{m\neq n}|P^S_{mn}|^2/M$, where the summations are restricted to *degenerate levels* for which $\omega_{mn}(B) = 0$. Here, the first term contributes to $MFE_M(B)$ response, whereas the second term contributes to the $MFE_{LC}(B)$ response that modulates $<\rho_S\ (t=\infty)>$ *primarily* at $B = 0$, where the singlet-triplet degeneracy is relatively high. The $MFE_M(B)$ response is monotonous due to the direct influence of *B*, and hence Zeeman effect in between the singlet-triplet PP spin mixing causing large field MFE. The $MFE_{LC}(B)$ component is caused by singlet-triplet level crossing and therefore has an *opposite* sign with respect to the regular $MFE_M(B)$ response, which results in a strong MFE(*B*) modulation response at $B = B_{LC}$. The combination of the monotonous $MFE_M(B)$ and $MFE_{LC}(B)$ components at *B*~0 explains, in principle, the USMFE response in organic devices.

When allowing for PP spin decay, $\rho_S(t)$ in Eq. (9) should then be revised to reflect the disappearance of PP with time. Furthermore, for MFE to occur, the decay rates of the singlet and triplet configuration must be different from one another. Thus, in a decaying system the population in each of the *M* levels would decay at a different rate γ_n for n = 1, …,*M*. Under these conditions, Eq. (9) for the singlet fraction is given by Ref. [71].

$$\rho_S(t) = Tr\left[\rho(t)P^S\right] = \frac{4}{M}\sum_{m,n=1}^{M}\left|P^S_{mn}\right|^2 \cos(\omega_{mn}t)e^{-\gamma_{nm}t}, \tag{10}$$

where $\gamma_{nm} = \gamma_n + \gamma_m$. Eq. (10) expresses that the singlet (or triplet) time evolution contains both a coherent character through the $cos(\omega_{nm}\ t)$ factor and an exponential decay factor. The measured MFE, that is MC and MEL, may be calculated using Eq. (10). For instance, if the dissociation yields are k_{SD} and k_{TD} for the singlet and triplet configurations, respectively, then the time dependent dissociated fraction of either the singlet or triplet is $k_{\alpha D}\rho_\alpha(t)$ (α = S,T) and thus the dissociation yield is [106].

$$\Phi_{\alpha D} = \int_0^\infty k_{\alpha D}\rho_\alpha(t)dt = \frac{4}{M}\sum_{n,m}P^\alpha_{n,m}\sigma_{m,n}(0)\frac{k_{\alpha D}\gamma_{nm}}{\gamma^2_{nm} + \omega^2_{nm}}. \tag{11}$$

The total dissociation yield is $\Phi_D = \Phi_{SD} + \Phi_{TD}$ and the *MC(B)* response is then given by

$$MC(B) = \frac{\Phi_D(B) - \Phi_D(0)}{\Phi_D(0)}. \tag{12}$$

For a slow decay such that $k << a_{HF}/\hbar$, the abrupt $MFE_{LC}(B)$ obtained at $B = 0$ in the absence of the spin decay is now spread over a field range of the order of $\hbar k/g\mu_B$, after which $\Phi_S(B)$ increases again due to the more dominant $MFE_M(B)$ component at large *B*.

For the MEL response, the final expression depends on the radiative recombination path of the singlet excitons (SE) and the detailed relaxation route from PP to the SE. As a result, PP^T (PP^S)

may transform not only to triplet exciton, TE, TE (SE) but also to SE (TE). Let us denote the effective SE (TE) generation rates, from the PP^{α} ($\alpha = S,T$) configuration, as $k_{\alpha,\mathrm{SE}}$ ($k_{\alpha,\mathrm{TE}}$). Then, similar to MC, we can define the "SE generation yield", $\Phi_{SE} = \Phi_{S,SE} + \Phi_{T,SE}$ where $\Phi_{\alpha,SE}$ is given by Eq. (11) in which $k_{\alpha D}$ is replaced by $k_{\alpha,\mathrm{SE}}$. Since the EL is proportional to the SE density, the MEL response is still given by Eq. (12), in which Φ_D is replaced by Φ_{SE}.

Fig. 12 shows the singlet yield and resulting MEL(B) response of the H-DOOPPV-based OLED. More importantly, the calculated MEL response captures the experimental USMEL response comprising of a negative component having minimum at B_{m} ~0.5 mT that changes sign to positive MEL with an approximate $B^2/(B_0^2+B^2)$ shape with $B_0 \approx 4.5$ mT. The high field shape, namely $B^2/(B_0^2+B^2)$, is a generic feature in this model. For small values of the exchange interaction, B_0 is determined primarily by the HFI constant a_{HF}; also the USMEL response is a strong function of the decay constant, k. The negative component with B_{min} appears only for relatively long decay times (e.g., $\hbar k/a_{HF} \leq 0.1$). For $J_{\mathrm{ex}}/a_{\mathrm{HF}} > 1$ the characteristic USMEL response is no longer distinguishable. More details about the calculation can be found in the literature [48,63,106].

In general, the PP model is widely used to explain the magnetic field effect in physics [70], chemistry and biology [71,72] and of course OMAR in OLEDs [55,63,82,87]. The general notion is that OMAR is large when both electrons and holes (or emission) are present in the device. We note that the direct observation of ISC in TADF materials in solid state has been recently achieved [107]. This further strengthens the model as a strong candidate for explaining OMAR. Nevertheless, it is not clear how this model can explain the MFE in unipolar devices where only one type of carriers exists. Since the impurity of OSCs is normally high, it is generally believed that the injected carriers can pair with opposite-sign charges from impurity and therefore the model is still able to explain OMAR in unipolar devices.

4.3. Triplet charge interaction model

Desai et al. [103] and Hu et al. [59] suggested the role played by triplets on the conducting charges of devices in order to explain OMAR. The model was first proposed by Ern and Merrifiel who used it to explain the MFE on triplet exciton quenching in organic crystals [108]. An exciton can transfer its energy to the ground state by interacting with either a free or trapped charge carrier. This interaction is more likely to happen with a triplet exciton because triplet lifetimes are a few orders of magnitude longer than singlet lifetimes. Therefore, the triplet density is dominant over the singlet density and is more likely to collide with charges.

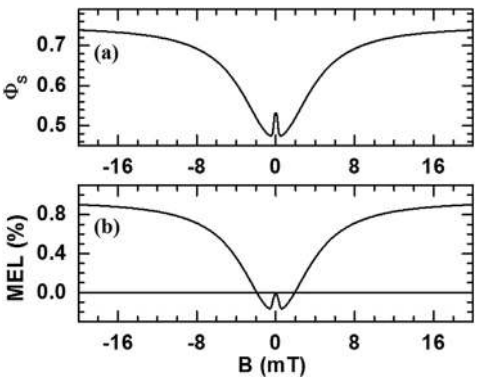

Fig. 12. Calculated magnetic field response of the singlet yield (a) and magneto-conductance (b) for a two-proton PP, where $g_1 = g_2 = g$ ~2, $a_1 = a_2 = a$, with $a/g\mu_B = 3.5$ mT, $J = 0$, $\delta_{\mathrm{TS}} = 0.96$ and $\hbar k/a = 2 \times 10^{-3}$. The resulting MEL response HWHM is ~4.5 mT, and B_{min} ~0.5 mT [48]. Reproduced with permission.

Desai et al. [56] used the model for the organic material Alq_3 in particular. Once turn-on voltage has been reached in an OLED, triplets are generated and, due to their long lifetime (estimated to be 25 μs in Alq_3), they will diffuse throughout the active layer until they spontaneously recombine or are quenched at the interfaces. Since triplets are neutral, the diffusion will be relatively slow and results in a large concentration of triplets being present in devices. Hence, their equilibrium concentration would be expected to increase with increasing current density. Based on the work by Ern and Merrifield [108], the triplets charge interaction with an estimated interaction radius of ~0.2 nm [109] can be written as:

$$T_1 + D_{\frac{1}{2}} \xleftarrow{k_1} \left(T_1 \ldots D_{\frac{1}{2}}\right) \xrightarrow{k_2} D_{\frac{1}{2}} + S_0^* \qquad (13)$$

where T_1 is the triplet exciton, $D_{\frac{1}{2}}$ is the spin 1/2 paramagnetic center, $\left(T_1 \ldots D_{\frac{1}{2}}\right)$ is a pair state, and k_1 is the rate of formation or backscattering from the pair state. The right hand side of the equation shows that the pair state can also dissociate into a free carrier and singlet ground state with a rate constant k_2, while releasing energy via phonons. The left-hand side of this equation describes a scattering event between a free carrier and a triplet, which will result in a decrease in the carrier mobility. In principle, k_1 depends on the density of polarons and triplet density while k_2 depends on the local magnetic field, including randomly oriented hyperfine fields. One can see that as the concentration of triplets decreases, the probability of scattering events decreases (smaller k_1) and hence the mobility should increase. Based on Desai et al. [56], since MEL is normally found to be positive, the magnetic field enhances the singlet density while diminishing the triplet density via ISC. Consequently, the triplet charge interaction becomes less effective and thereby enhances the mobility of the OLED leading to positive MFE.

Hu et al. [59] suggested two competing mechanisms in which MC can be negative or positive: (i) Since the singlet excitons have a smaller ionic nature than triplet excitons, when EL increases, the dissociation of singlet excitons into free charges also increases. This leads to positive MEL and MC. In addition, triplet excitons can collide and transfer their energy to trapped polarons to increase free polaron density by detrapping the trapped polarons, leading to positive MC. (ii) The negative MC comes from the argument that magnetic fields can slow down the triplet-charge interaction process (smaller k_2 in Eq. (13)) leading to smaller free polarons releasing from this reaction. By controlling the negative to positive polaron density ratio in OLEDs, Hu et al. effectively changed the sign of MC inside the devices. We note that recently using microscopic and numerical device simulations, Janssen et al. showed that this model can reproduce the important features of OMAR [110].

In principle, the model can be used to explain the OMAR sign change and line shape of OMAR. However, this model predicts that OMAR should increase with increasing current density or triplet charge collision. This is, in fact, not the case as OMAR has its largest value at relative low current density [83]. In addition, Geng et al. shows that OMAR magnitude decreases when the photo-excited exciton density increases, contrary with the model prediction [61,111].

4.4. Δg mechanism

The Δg mechanism was first proposed by Wang et al. [112] to explain the MFE in MEH-PPV/fullerene blend OLEDs. The blend is normally used in organic photovoltaics in which the charge separation is one of important factors for the operation of the device.

The magnetic field acts on charge transfer states (exciplex) where an electron localized at the fullerene acceptor has different g factor (g^-) than a hole (g^+) localized in MEH-PPV donor. Based on the Δg mechanism, the singlet and triplet spin mixing rate is proportional to the difference of the electron and hole Larmor frequency, which can be described as $\Delta g\mu_B B$. In principle, spin mixing needs to satisfy both conservation of spin momentum and energy. The spin can be conserved by either exchange with nuclear spin (HFI of PP mechanism) or local magnetic field via Δg mechanism. The energy of the singlet and triplet states can be modified by emitting or absorbing phonons as in the case of TADF. At low magnetic field, since the Zeeman splitting is small, the spin mixing is more effective and can be governed by both HFI and the Δg mechanisms. At high magnetic field, the Zeeman energy is large and the spin mixing by HFI becomes less influential, while the spin mixing rate caused by the Δg mechanism increases. Consequently, the dependence of MFE on the magnetic field becomes less effective at high field. Fig. 13a shows that the interconversion between singlet and triplet states is affected by the Zeeman splitting while Fig. 13b describes the MFE caused by Δg mechanism. If applied magnetic field is large, there are only spin mixing between singlet, S and triplet, T_0 (with zero projection spin in the quantization axis) is effective. The detailed calculation when Δg term is included into the PP Hamiltonian can be found in the literature [68,69]. The model has been considered as a main mechanism for the giant OMAR effect on TADF-based OLEDs [69]. However, recent MFE study on transient photoluminescence of the same TADF blend shows compelling evidence that PP mechanism is still a dominant mechanism in such compound [113]. Since the Δg model is the newest one among OMAR models, more experiments need to be done to verify its accuracy.

5. Summary and outlook

We summarized all prominent experimental results of OMAR in OLEDs and organic unipolar devices. We addressed four different mechanisms for explaining OMAR effect. There is not yet a consensus on the leading model for OMAR in organic devices since none of the existing models can be used to confidently explain all cases of OMAR response. Therefore, MFE in OLEDs is still an attractive topic for debate. Nevertheless, it is widely accepted that random hyperfine fields play a central role in the MFE response, which exists in all the models except the Δg mechanism. The multiple components in the OMAR response might imply that more than one mechanism occurs simultaneously. Since MFE in OLEDs is large at room temperature, it has a great potential for magnetic sensor and lighting applications. The recent discovery of giant OMAR in TADF-based OLEDs is very promising for the advancement of such applications in the near future. So far, MFE studies using TADF materials are very limited. The OMAR mechanism behind this astonishing effect is still unclear due to lack of experimental evidence. For example, it is not clear how the OMAR response occurs when the exchange energy gradually changes. Finally, all OMAR studies thus far are done in large area OLEDs of about 1 mm^2, where the capacitance of the device is large leading to slow response time of the device. OMAR studies on nanoscale OLEDs would simplify the spin dynamics in OLEDs for a better understanding of OMAR. In addition, owning to a much smaller capacitance, a nanometer OMAR device might have a fast response time for critical applications such as fast light sources for fiber-optic telecommunications.

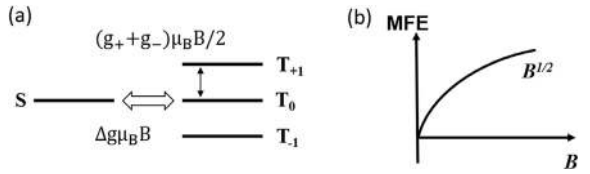

Fig. 13. (a) Schematic of Δg mechanism where the spin mixing rate, $\Delta g\mu_B B$ between singlet and triplet manifold are shown. (b) General behavior of MFE with applied magnetic field.

Acknowledgments

We acknowledge the University of Georgia start-up funds and Faculty Research Grant (UGAFR-FRG 064100291) for funding this work. This paper belongs to the special issue for a memory of Dr. Peter Brommer - a former physicist of the University of Amsterdam.

References

[1] S.A. Wolf, D.D. Awschalom, R.A. Buhrman, J.M. Daughton, S. von Molnar, M.L. Roukes, A.Y. Chtchelkanova, D.M. Treger, Spintronics: a spin-based electronics vision for the future, Science 294 (2001) 1488–1495.
[2] I. Zutic, J. Fabian, a.S. Das-Sarma, Spintronics: fundamentals and applications, Revew Mod. Phys. 76 (2004) 323–410.
[3] W. Gerlach, O. Stern, Das magnetische moment des silberatoms, Z. Phys. 9 (1922) 353–355.
[4] W. Gerlach, O. Stern, Der experimentelle Nachweis der Richtungsquantelung im Magnetfeld, Z. Phys. 9 (1922) 349–352.
[5] I.I. Rabi, J.R. Zacharias, S. Millman, P. Kusch, A new method of measuring nuclear magnetic moment, Phys. Rev. 53 (1938), 318–318.
[6] M. Julliere, Tunneling between ferromagnetic-films, Phys. Lett. A 54 (1975) 225–226.
[7] P.M. Tedrow, R. Meservey, Spin polarization of electrons tunneling from films of Fe, Co, Ni, and Gd, Phys. Rev. B 7 (1973) 318–326.
[8] C. Chappert, A. Fert, F.N. Van Dau, The emergence of spin electronics in data storage, Nat. Mater. 6 (2007) 813–823.
[9] M. Baibich, J.M. Broto, A. Fert, F. NguyenVanDan, F. Petroff, P. Etienne, G. Creuzert, A. Friederich, J. Chazelas, Giant magnetoresistance of (001)Fe/(001)Cr magnetic superlattices, Phys. Rev. Lett. 61 (1988) 2472–2475.
[10] G. Binasch, P. Grunberg, F. Saurenbach, W. Zinn, Enhanced magnetoresistance in layered magnetic-structures with antiferromagnetic interlayer exchange, Phys. Rev. B 39 (1989) 4828–4830.
[11] Y. Tian, S. Yan, Giant magnetoresistance: history, development and beyond, Sci. China Phys. Mech. Astron. 56 (2013) 2–14.
[12] S.S.P. Parkin, Giant magnetoresistance in magnetic nanostructures, Annu. Rev. Mater Sci. 25 (1995) 357–388.
[13] K. Taguchi, T. Yokoyama, Y. Tanaka, Giant magnetoresistance in the junction of two ferromagnets on the surface of diffusive topological insulators, Phys. Rev. B 89 (2014) 085407.
[14] J.P. Velev, C.-G. Duan, J.D. Burton, A. Smogunov, M.K. Niranjan, E. Tosatti, S.S. Jaswal, E.Y. Tsymbal, Magnetic tunnel junctions with ferroelectric barriers: prediction of four resistance states from first principles, Nano Lett. 9 (2009) 427–432.
[15] G. Schmidt, Concepts for spin injection into semiconductors - a review, J. Phys. D. Appl. Phys. 38 (2005) R107–R122.
[16] F.J. Jedema, A.T. Filip, B.J. van Wees, Electrical spin injection and accumulation at room temperature in an all-metal mesoscopic spin valve, Nature 410 (2001) 345–348.
[17] C.N.R. Rao, A.K. Cheetham, Giant magnetoresistance in transition metal oxides, Science 272 (1996) 369–370.
[18] A.A. Baker, A.I. Figueroa, L.J. Collins-McIntyre, G. van der Laan, T. Hesjedal, Spin pumping in ferromagnet-topological insulator-ferromagnet heterostructures, Sci. Rep. 5 (2015) 7907.
[19] S.Z. Peng, Y. Zhang, M.X. Wang, Y.G. Zhang, W. Zhao, J.G. Webster, Magnetic Tunnel Junctions for Spintronics: Principles and Applications, Wiley Encyclopedia of Electrical and Electronics Engineering, John Wiley & Sons, Inc, 1999.
[20] W.J.M. Naber, S. Faez, W.G. van der Wiel, Organic spintronics, J. Phys. D. 40 (2007) R205–R228.
[21] V. Dediu, M. Murgia, F.C. Matacotta, C. Taliani, S. Barbanera, Room temperature spin polarized injection in organic semiconductor, Solid State Commun. 122 (2002) 181–184.
[22] Z.H. Xiong, D. Wu, Z.V. Vardeny, J. Shi, Giant magnetoresistance in organic spin-valves, Nature 427 (2004) 821–824.
[23] X. Lou, C. Adelmann, S.A. Crooker, E.S. Garlid, J. Zhang, K.S.M. Reddy, S.D. Flexner, C.J. Palmstrom, P.A. Crowell, Electrical detection of spin transport in lateral ferromagnet-semiconductor devices, Nat. Phys. 3 (2007) 197–202.
[24] J.H. Burroughes, D.D.C. Bradley, A.R. Brown, R.N. Marks, K. Mackay, R.H. Friend, P.L. Burn, A.B. Holmes, Light-emitting-diodes based on conjugated polymers, Nature 347 (1990) 539–541.
[25] C.W. Tang, S.A. VanSlyke, Organic electroluminescent diodes, Appl. Phys. Lett. 51 (1987) 913–915.

Please cite this article in press as: R. Geng, et al., A review on organic spintronic materials and devices: I. Magnetic field effect on organic light emitting diodes, Journal of Science: Advanced Materials and Devices (2016), http://dx.doi.org/10.1016/j.jsamd.2016.05.002

[26] B.W. D'Andrade, S.R. Forrest, White organic light-emitting devices for solid-state lighting, Adv. Mater 16 (2004) 1585–1595.
[27] C.W. Tang, 2-layer organic photovoltaic cell, Appl. Phys. Lett. 48 (1986) 183–185.
[28] A.J. Heeger, 25th anniversary article: bulk heterojunction solar cells: understanding the mechanism of operation, Adv. Mater. 26 (2014) 10–28.
[29] A. Tsumura, H. Koezuka, T. Ando, Macromolecular electronic device: field-effect transistor with a polythiophene thin film, Appl. Phys. Lett. 49 (1986) 1210–1212.
[30] C.D. Dimitrakopoulos, P.R.L. Malenfant, Organic thin film transistors for large area electronics, Adv. Mater. 14 (2002) 99–117.
[31] S. Reineke, M. Thomschke, B. Lüssem, K. Leo, White organic light-emitting diodes: status and perspective, Rev. Mod. Phys. 85 (2013) 1245–1293.
[32] V.A. Dediu, L.E. Hueso, I. Bergenti, C. Taliani, Spin routes in organic semiconductors, Nat. Mater. 8 (2009) 707–716.
[33] T.D. Nguyen, E. Ehrenfreund, Z.V. Vardeny, Spin-polarized light-emitting diode based on an organic bipolar spin valve, Science 337 (2012) 204–209.
[34] D. Sun, L. Yin, C. Sun, H. Guo, Z. Gai, X.G. Zhang, T.Z. Ward, Z. Cheng, J. Shen, Giant magnetoresistance in organic spin valves, Phys. Rev. Lett. 104 (2010) 236602.
[35] F. Wang, Z.V. Vardeny, Recent advances in organic spin-valve devices, Synth. Met. 160 (2010) 210–215.
[36] H. Shirakawa, E.J. Louis, A.G. MacDiarmid, C.K. Chiang, A.J. Heeger, Synthesis of electrically conducting organic polymers: halogen derivatives of polyacetylene, (CH), J. Chem. Soc. Chem. Commun. (1977) 578–580.
[37] V. Coropceanu, J. Cornil, D.A. da Silva Filho, Y. Olivier, R. Silbey, J.-L. Brédas, Charge transport in organic semiconductors, Chem. Rev. 107 (2007) 926–952.
[38] J. Fabian, A. Matos-Abiague, C. Ertler, P. Stano, I. Zutic, Semiconductor spintronics, Acta Phys. Slovaca 57 (2007) 565.
[39] L.D. Landau, E.M. Lifshitz, Quantum mechanics: non relativistic theory, Pergamon Press Plc, Headington Hill Hall, Oxford OX3 OBW, England, 1977.
[40] S. Sanvito, Molecular spintronics, Chem. Soc. Rev. 40 (2011) 3336–3355.
[41] S. Datta, B. Das, Electronic analog of the electro-optic modulator, Appl. Phys. Lett. 56 (1990) 665–667.
[42] A.J. Drew, J. Hoppler, L. Schulz, F.L. Pratt, P. Desai, P. Shakya, T. Kreouzis, W.P. Gillin, A. Suter, N.A. Morley, V.K. Malik, A. Dubroka, K.W. Kim, H. Bouyanfif, F. Bourqui, C. Bernhard, R. Scheuermann, G.J. Nieuwenhuys, T. Prokscha, E. Morenzoni, Direct measurement of the electronic spin diffusion length in a fully functional organic spin valve by low-energy muon spin rotation, Nat. Mater. 8 (2009) 109–114.
[43] M. Cinchetti, K. Heimer, J. Wüstenberg, O. Andreyev, M. Bauer, S. Lach, C. Ziegler, Y. Gao, M. Aeschlimann, Determination of spin injection and transport in a ferromagnet/organic semiconductor heterojunction by two-photon photoemission, Nat. Mater. 8 (2009) 115–119.
[44] J.F. Ren, J.Y. Fu, D.S. Liu, L.M. Mei, S.J. Xie, Diffusion theory of spin injection into organic polymers, J. Phys. Condens. Matter 17 (2005) 2341–2347.
[45] Z.G. Yu, Suppression of the Hanle effect in organic spintronic devices, Phys. Rev. Lett. 111 (2013) 016601.
[46] W. Xu, G.J. Szulczewski, P. LeClair, I. Navarrete, R. Schad, G.X. Miao, H. Guo, A. Gupta, Tunneling magnetoresistance observed in La0.67Sr0.33MnO3/organic molecule/Co junctions, Appl. Phys. Lett. 90 (2007) 072506.
[47] M. Grünewald, R. Göckeritz, N. Homonnay, F. Würthner, L.W. Molenkamp, G. Schmidt, Vertical organic spin valves in perpendicular magnetic fields, Phys. Rev. B 88 (2013) 085319.
[48] T.D. Nguyen, G. Hukic-Markosian, F. Wang, L. Wojcik, X. Li, E. Ehrenfreund, Z.V. Vardeny, Isotope effect in spin response of [pi]-conjugated polymer films and devices, Nat. Mater. 9 (2010) 345–352.
[49] W. Wagemans, B. Koopmans, Spin transport and magnetoresistance in organic semiconductors, Phys. Status Solidi B 248 (2011) 1029–1041.
[50] D.L. Sun, E. Ehrenfreund, Z.V. Vardeny, The first decade of organic spintronics research, Chem. Commun. 50 (2014) 1781–1793.
[51] C. Barraud, P. Seneor, R. Mattana, S. Fusil, K. Bouzehouane, C. Deranlot, P. Graziosi, L. Hueso, I. Bergenti, V. Dediu, F. Petroff, A. Fert, Unravelling the role of the interface for spin injection into organic semiconductors, Nat. Phys. 6 (2010) 615–620.
[52] M. Wohlgenannt, Organic magnetoresistance and spin diffusion in organic semiconductor thin film devices, Phys. status solidi (RRL) – Rapid Res. Lett. 6 (2012) 229–242.
[53] T.D. Nguyen, Y. Sheng, J. Rybicki, G. Veeraraghavan, M. Wohlgenannt, Magnetoresistance in π-conjugated organic sandwich devices with varying hyperfine and spin-orbit coupling strengths, and varying dopant concentrations, J. Mater. Chem. 17 (2007) 1995–2001.
[54] O. Mermer, G. Veeraraghavan, T.L. Francis, Y. Sheng, D.T. Nguyen, M. Wohlgenannt, A. Kohler, M.K. Al-Suti, M.S. Khan, Large magnetoresistance in nonmagnetic π-conjugated semiconductor thin film devices, Phys. Rev. B 72 (2005) 205202.
[55] V.N. Prigodin, J.D. Bergeson, D.M. Lincoln, A.J. Epstein, Anomalous room temperature magnetoresistance in organic semiconductors, Synth. Met. 156 (2006) 757–761.
[56] P. Desai, P. Shakya, T. Kreouzis, W.P. Gillin, N.A. Morley, M.R.J. Gibbs, Magnetoresistance and efficiency measurements of Alq3-based OLEDs, Phys. Rev. B 75 (2007) 094423.
[57] P.A. Bobbert, T.D. Nguyen, F.W.A. van Oost, B. Koopmans, M. Wohlgenannt, Bipolaron mechanism for organic magnetoresistance, Phys. Rev. Lett. 99 (2007) 216801.
[58] F.L. Bloom, W. Wagemans, M. Kemerink, B. Koopmans, Separating positive and negative magnetoresistance in organic semiconductor devices, Phys. Rev. Lett. 99 (2007) 257201.
[59] B. Hu, Y. Wu, Tuning magnetoresistance between positive and negative values in organic semiconductors, Nat. Mater. 6 (2007) 985–991.
[60] F.J. Wang, H. Bassler, Z.V. Vardeny, Magnetic field effects in π-conjugated polymer-fullerene blends: evidence for multiple components, Phys. Rev. Lett. 101 (2008) 236805.
[61] R. Geng, N.T. Mayhew, T.D. Nguyen, Tunable magneto-conductance and magneto-electroluminescence in polymer light-emitting electrochemical planar devices, Appl. Phys. Lett. 103 (2013) 243307.
[62] J. Kalinowski, J. Szmytkowski, W. Stampor, Magnetic hyperfine modulation of charge photogeneration in solid films of Alq_3, Chem. Phys. Lett. 378 (2003) 380–387.
[63] T.D. Nguyen, B.R. Gautam, E. Ehrenfreund, Z.V. Vardeny, Magneto-conductance response in unipolar and bipolar organic diodes at ultrasmall fields, Phys. Rev. Lett. 105 (2010) 166804.
[64] T.D. Nguyen, G. Hukic-Markosian, F.J. Wang, L. Wojcik, X.G. Li, E. Ehrenfreund, Z.V. Vardeny, The hyperfine interaction role in the spin response of pi-conjugated polymer films and spin valve devices, Synth. Met. 161 (2011) 598–603.
[65] Y. Sheng, T.D. Nguyen, G. Veeraraghavan, Ö. Mermer, M. Wohlgenannt, S. Qiu, U. Scherf, Hyperfine interaction and magnetoresistance in organic semiconductors, Phys. Rev. B 74 (2006) 045213.
[66] P. Shakya, P. Desai, M. Somerton, G. Gannaway, T. Kreouzis, W.P. Gillin, The magnetic field effect on the transport and efficiency of group III tris(8-hydroxyquinoline) organic light emitting diodes, J. Appl. Phys. 103 (2008) 103715.
[67] L. Nuccio, M. Willis, L. Schulz, S. Fratini, F. Messina, M. D'Amico, F.L. Pratt, J.S. Lord, I. McKenzie, M. Loth, B. Purushothaman, J. Anthony, M. Heeney, R.M. Wilson, I. Hernandez, M. Cannas, K. Sedlak, T. Kreouzis, W.P. Gillin, C. Bernhard, A.J. Drew, Importance of spin-orbit interaction for the electron spin relaxation in organic semiconductors, Phys. Rev. Lett. 110 (2013) 216602.
[68] A.H. Devir-Wolfman, B. Khachatryan, B.R. Gautam, L. Tzabary, A. Keren, N. Tessler, Z.V. Vardeny, E. Ehrenfreund, Short-lived charge-transfer excitons in organic photovoltaic cells studied by high-field magneto-photocurrent, Nat. Commun. 5 (2014).
[69] Y. Wang, K. Sahin-Tiras, N.J. Harmon, M. Wohlgenannt, M.E. Flatté, Immense magnetic response of exciplex light emission due to correlated spin-charge dynamics, Phys. Rev. X 6 (2016) 011011.
[70] R.P. Groff, A. Suna, P. Avakian, R.E. Merrifield, Magnetic hyperfine modulation of dye-sensitized delayed fluorescence in organic crystals, Phys. Rev. B 9 (1974) 2655–2660.
[71] C.R. Timmel, Effects of weak magnetic fields on free radical recombination reactions, Mol. Phys. 95 (1998) 71–89.
[72] H. Hayashi, Introduction to dynamic spin chemistry; magnetic field effects on chemical and biochemical reactions, World Scientific Publishing, 2004. World Scientific Lecture and Course Notes in Chemistry.
[73] V.N. Prigodin, J.W. Yoo, H.W. Jang, C. Kao, C.B. Eom, A.J. Epstein, New advances in organic spintronics, J. Phys. Conf. Ser. 292 (2011) 012001.
[74] J.M. Lupton, D.R. McCamey, C. Boehme, Coherent spin manipulation in molecular semiconductors: getting a handle on organic spintronics, ChemPhysChem 11 (2010) 3040–3058.
[75] T.D. Nguyen, E. Ehrenfreund, Z.V. Vardeny, The development of organic spin valves from unipolar to bipolar operation, MRS Bull. 39 (2014) 585–589.
[76] A.J. Drew, G. Szulczewski, L. Nuccio, W.P. Gillin, The role of interfaces in organic spin valves revealed through spectroscopic and transport measurements, Phys. status solidi (b) 249 (2012) 9–17.
[77] J. Devkota, R. Geng, R.C. Subedi, T.D. Nguyen, Organic spin valves: a review, Adv. Funct. Mater. (2016) http://dx.doi.org/10.1002/adfm.201504209.
[78] B. Hu, L. Yan, M. Shao, Magnetic-field effects in organic semiconducting materials and devices, Adv. Mater. 21 (2009) 1500–1516.
[79] M.A. Baldo, D.F. O'Brien, Y. You, A. Shoustikov, S. Sibley, M.E. Thompson, S.R. Forrest, Highly efficient phosphorescent emission from organic electroluminescent devices, Nature 395 (1998) 151–154.
[80] H. Uoyama, K. Goushi, K. Shizu, H. Nomura, C. Adachi, Highly efficient organic light-emitting diodes from delayed fluorescence, Nature 492 (2012) 234–238.
[81] F.B. Dias, K.N. Bourdakos, V. Jankus, K.C. Moss, K.T. Kamtekar, V. Bhalla, J. Santos, M.R. Bryce, A.P. Monkman, Triplet harvesting with 100% efficiency by way of thermally activated delayed fluorescence in charge transfer OLED emitters, Adv. Mater. 25 (2013) 3707–3714.
[82] J. Kalinowski, M. Cocchi, D. Virgili, V. Fattori, P.D. Marco, Magnetic field effects on organic electrophosphorescence, Phys. Rev. B 70 (2004) 205303–205309.
[83] T.L. Francis, O. Mermer, G. Veeraraghavan, M. Wohlgenannt, Large magnetoresistance at room-temperature in small-molecular weight organic semiconductor sandwich devices, New J. Phys. 6 (2004) 185–192.
[84] E.L. Frankevich, A.A. Lymarev, I. Sokolik, F.E. Karasz, S. Blumstengel, R.H. Baughman, H.H. Hörhold, Polaron-pair generation in poly(phenylene vinylenes), Phys. Rev. B 46 (1992) 9320–9324.
[85] T.D. Nguyen, Y. Sheng, J. Rybicki, M. Wohlgenannt, Magnetic field-effects in bipolar, almost hole-only and almost electron-only tris-(8-hydroxyquinoline) aluminum devices, Phys. Rev. B 77 (2008) 235209–235215.

Please cite this article in press as: R. Geng, et al., A review on organic spintronic materials and devices: I. Magnetic field effect on organic light emitting diodes, Journal of Science: Advanced Materials and Devices (2016), http://dx.doi.org/10.1016/j.jsamd.2016.05.002

[86] Y. Ling, Y. Lei, Q. Zhang, L. Chen, Q. Song, Z. Xiong, Large magneto-conductance and magneto-electroluminescence in exciplex-based organic light-emitting diodes at room temperature, Appl. Phys. Lett. 107 (2015) 213301.
[87] J.D. Bergeson, V.N. Prigodin, D.M. Lincoln, A.J. Epstein, Inversion of magnetoresistance in organic semiconductors, Phys. Rev. Lett. 100 (2008) 067201.
[88] U. Niedermeier, M. Vieth, R. Pätzold, W. Sarfert, H.v. Seggern, Enhancement of organic magnetoresistance by electrical conditioning, Appl. Phys. Lett. 92 (2008) 193309–193312.
[89] J. Rybicki, R. Lin, F. Wang, M. Wohlgenannt, C. He, T. Sanders, Y. Suzuki, Tuning the performance of organic spintronic devices using X-ray generated traps, Phys. Rev. Lett. 109 (2012) 076603.
[90] S. Zhang, A.J. Drew, T. Kreouzis, W.P. Gillin, Modelling of organic magnetoresistance as a function of temperature using the triplet polaron interaction, Synth. Met. 161 (2011) 628–631.
[91] N.J. Rolfe, M. Heeney, P.B. Wyatt, A.J. Drew, T. Kreouzis, W.P. Gillin, The effect of deuteration on organic magnetoresistance, Synth. Met. 161 (2011) 608–612.
[92] F.L. Bloom, M. Kemerink, W. Wagemans, B. Koopmans, Sign inversion of magnetoresistance in space-charge limited organic devices, Phys. Rev. Lett. 103 (2009) 066601–066604.
[93] N.J. Rolfe, M. Heeney, P.B. Wyatt, A.J. Drew, T. Kreouzis, W.P. Gillin, Elucidating the role of hyperfine interactions on organic magnetoresistance using deuterated aluminium tris(8-hydroxyquinoline), Phys. Rev. B 80 (2009) 241201.
[94] T.D. Nguyen, T.P. Basel, Y.J. Pu, X.G. Li, E. Ehrenfreund, Z.V. Vardeny, Isotope effect in the spin response of aluminum tris(8-hydroxyquinoline) based devices, Phys. Rev. B 85 (2012) 245437.
[95] M. Cölle, C. Gärditz, Delayed fluorescence and phosphorescence of tris-(8-hydroxyquinoline)aluminum (Alq_3) and their temperature dependence, J. Luminescence 110 (2004) 200–206.
[96] T.D. Nguyen, Y. Sheng, M. Wohlgenannt, T.D. Anthopoulos, On the role of hydrogen in organic magnetoresistance: a study of C_{60} devices, Synth. Met. 157 (2007) 930–934.
[97] H. Malissa, M. Kavand, D.P. Waters, K.J. van Schooten, P.L. Burn, Z.V. Vardeny, B. Saam, J.M. Lupton, C. Boehme, Room-temperature coupling between electrical current and nuclear spins in OLEDs, Science 345 (2014) 1487–1490.
[98] B. Brocklehurst, K.A. McLauchlan, Free radical mechanism for the effects of environmental electromagnetic fields on biological systems, Int. J. Radiat. Biol. 69 (1996) 3–24.
[99] R. Belaid, T. Barhoumi, L. Hachani, L. Hassine, H. Bouchriha, Magnetic field effect on recombination light in anthracene crystal, Synth. Met. 131 (2002) 23–30.
[100] D.R. McCamey, K.J. van Schooten, W.J. Baker, S.Y. Lee, S.Y. Paik, J.M. Lupton, C. Boehme, Hyperfine-field-mediated spin beating in electrostatically bound charge carrier pairs, Phys. Rev. Lett. 104 (2010) 017601.
[101] Y. Sheng, T.D. Nguyen, G. Veeraraghavan, O. Mermer, M. Wohlgenannt, Effect of spin-orbit coupling on magnetoresistance in organic semiconductors, Phys. Rev. B 75 (2007) 035202.
[102] S. Liang, R. Geng, B. Yang, W. Zhao, R. Chandra Subedi, X. Li, X. Han, T.D. Nguyen, Curvature-enhanced spin-orbit coupling and spinterface effect in fullerene-based spin valves, Sci. Rep. 6 (2016) 19461.
[103] P. Desai, P. Shakya, T. Kreouzis, W.P. Gillin, Magnetoresistance in organic light-emitting diode structures under illumination, Phys. Rev. B 76 (2007) 235202.
[104] N.J. Harmon, M.E. Flatté, Spin-flip induced magnetoresistance in positionally disordered organic solids, Phys. Rev. Lett. 108 (2012) 186602–186605.
[105] R.N. Mahato, H. Lülf, M.H. Siekman, S.P. Kersten, P.A. Bobbert, M.P. de Jong, L. De Cola, W.G. van der Wiel, Ultrahigh magnetoresistance at room temperature in molecular wires, Science 341 (2013) 257–260.
[106] E. Ehrenfreund, Z.V. Vardeny, Effects of magnetic field on conductance and electroluminescence in organic devices, Israel J. Chem. 52 (2012) 552–562.
[107] L. Bergmann, G.J. Hedley, T. Baumann, S. Bräse, I.D.W. Samuel, Direct observation of intersystem crossing in a thermally activated delayed fluorescence copper complex in the solid state, Sci. Adv. 2 (2016).
[108] V. Ern, R.E. Merrifield, Magnetic field effect on triplet exciton quenching in organic crystals, Phys. Rev. Lett. 21 (1968) 609–611.
[109] D. Hertel, K. Meerholz, Triplet-polaron quenching in conjugated polymers, J. Phys. Chem. B 111 (2007) 12075–12080.
[110] P. Janssen, M. Cox, S.H.W. Wouters, M. Kemerink, M.M. Wienk, B. Koopmans, Tuning organic magnetoresistance in polymer-fullerene blends by controlling spin reaction pathways, Nat. Commun. (2013) 2286.
[111] R. Geng, R.C. Subedi, S. Liang, T.D. Nguyen, Discernment of possible organic magnetic field effect machanisms using polymer light-emitting electrochemical cells, SPIN 04 (2014) 1440010.
[112] F. Wang, H. Bassler, Z.V. Vardeny, Studies of magnetoresistance in polymer/fullerene blends, Phys. Rev. Lett. 101 (2008) 236805–236808.
[113] E. Hontz, W. Chang, D.N. Congreve, V. Bulović, M.A. Baldo, T. Van Voorhis, The role of electron–hole separation in thermally activated delayed fluorescence in donor–acceptor blends, J. Phys. Chem. C 119 (2015) 25591–25597.

Please cite this article in press as: R. Geng, et al., A review on organic spintronic materials and devices: I. Magnetic field effect on organic light emitting diodes, Journal of Science: Advanced Materials and Devices (2016), http://dx.doi.org/10.1016/j.jsamd.2016.05.002